



## RGB SAR products: methods and applications

**Donato Amitrano\***, Gerardo Di Martino, Antonio Iodice,  
Daniele Riccio and Giuseppe Ruello

University of Napoli Federico II, Via Claudio 21, 80125, Napoli, Italy

\*Corresponding author, e-mail address: donato.amitrano@unina.it

### Abstract

In this paper, we introduce a new framework for the RGB representation of SAR data. The purpose is to lower the expertise required to manage data, providing intermediate products between the classic Level-1 and Level-2. These products are particularly oriented toward the end-user community. In fact, their principal characteristics are interpretability, reproducibility and possibility to be processed with simple algorithms, widely available in the most popular software suites. The proposed framework and products are discussed through examples in which the above-mentioned properties are highlighted. Finally, their suitability in applicative contexts is demonstrated through two examples concerning classification activities, implemented exploiting both pixel-based and object-based techniques.

**Keywords:** SAR, multitemporal, classification, OBIA, RGB, change-detection.

### Introduction

Reconstruction of the world for data analysis, monitoring, planning, and response to natural hazards is the principal purpose of sensing. To this end, several sensors can be exploited, often acquiring data outside the visible spectrum. In these cases, the human-machine interface is fundamental to fully understand data, especially in a multi-disciplinary environment, where scientists with different background collaborate to the information extraction process.

Remote sensing scientists retrieve from a picture the physical information they are looking for. However, the extraction of information through a machine is not so easy as the interpretation of real world images is for humans. Campbell and Wynne, at the beginning of their *Introduction on Remote Sensing* clarify this concept:

*“Pictures concisely convey information about positions, sizes, and interrelationships between objects. [...] humans possess a high level of proficiency in deriving information from such images, (therefore) we experience little difficulty in interpreting even those scenes that are visually complex. We are so competent in such task that it is only when we attempt to replicate these capabilities using computer programs [...] that we realize how powerful our abilities are [...]”* [Campbell and Wynne, 2011].

This sentence highlights the proficiency of humans in image interpretation and the difficulty we find trying to reproduce our vision mechanism on a machine (see Marr [1982] for a complete discussion about machine vision). However, dealing with images acquired outside the visible spectrum, the information mining could be difficult even at visual level, since the operator (unless he/she has a significant expertise with that particular sensor) has no experience of the reality as filtered by the sensor. Therefore, an effort must be made to make data understandable by users, which often have a limited technical expertise.

The second, and last, sentence we report is a definition of remote sensing:

*“Remote sensing has been variously defined but basically it is the art or science of telling something about an object without touching it”* [Fischer et al., 1976].

It has been extracted from a very old paper, but we think it is very significant because it introduces the concept of remote sensing as science, of course, but also the art of telling a story about an object. This is the principal purpose of using images, which are a mean to immediately transfer information and feelings to their observer.

One of the issues preventing the diffusion of SAR data is that their standard appearance is quite unpleasant. In fact, if one looks at the picture reported in Figure 1, representing a standard single look SAR image shot on a rural area of Burkina Faso (western Africa), it is rather clear that the extraction of information is difficult, even for users with high expertise with radar imaging.

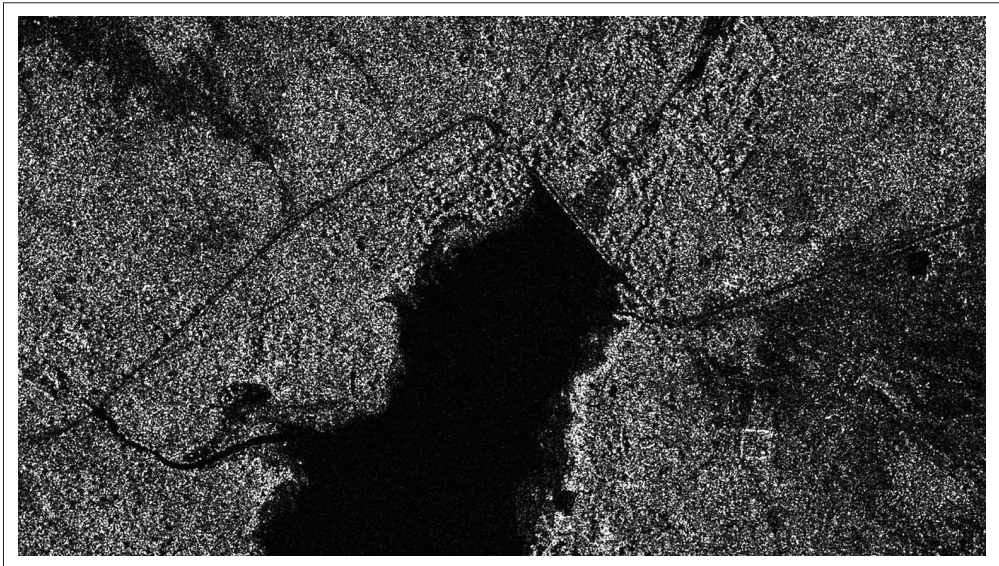


**Figure 1 - Burkina Faso, COSMO-SkyMed SLC SAR product.**

Some basic operations for enhancing the interpretability of images can be implanted. Despeckling, for example, is a common practice to enhance SAR images appearance and improve interpretability [Di Martino et al., 2014]. In Figure 2, we display the same product of Figure 1 after multitemporal De Grandi speckle filtering [De Grandi et al., 1997] using

about 30 images. This image is more easily understandable, at least for people having a technical expertise with SAR imagery.

It is quite clear that one of the most annoying problems handling SAR data is the grayscale displaying, having humans the habit to deal with color images [Jacobson et al., 2007], [Amitrano et al., 2016]. This scenario is further complicated by the scarce availability of commercial/open source software suites implementing *ad hoc* algorithms for data analysis. The result is that, usually, end-users prefer to deal with data they can handle more easily (optical, multispectral, orthophoto).

We think that an effort is necessary, in the SAR community, to favor the diffusion of data toward the general public. Indeed, this is possible by developing more user-oriented processing chains [Madhok and Landgrebe, 2002; Datcu and Seidel, 2005; Amitrano et al., 2015; Amitrano et al., 2016b]. In this paper, we introduce a framework designed to satisfy some fundamental end-user requirements, such as interpretability, repeatability, possibility to extract information with simple algorithms, and robustness with respect to variations of sensors and/or scene.



**Figure 2 - Burkina Faso, COSMO-SkyMed product after multitemporal De Grandi despeckling.**

### Framework and products

In Figure 3, the general scheme of the proposed framework (we called MAP3) is depicted (see Amitrano et al., [2015] and Amitrano et al. [2016] for details). It is composed by three blocks of activities: pre-processing chain, adaptive processing chain and representation/analysis chain. Each block is composed by a sequence of simple operations, very well documented in literature. As an example, for data calibration, the reader can refer to Infoterra [2014], for the calibration of TerraSAR-X data. Multitemporal despeckling is proposed to preserve the spatial resolution. Available algorithms on free or commercial software suites

have been presented in De Grandi et al. [1997] and Martinez and Le Toan [2007]. Cross-calibration/normalization is fundamental for making SAR images (characterized by exponential pdf) suitable to be displayed on linear scale in RGB combination. Solutions to this problem can be found in Dellepiane and Angiati [2012] and Amitrano et al. [2015].

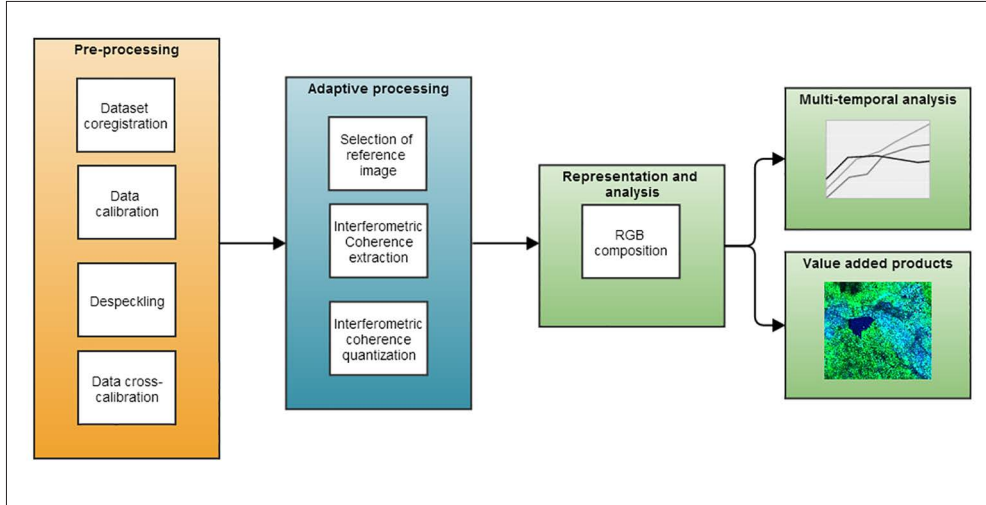


**Figure 3 - General schema of the MAP3 framework.**

The proposed framework has three fundamental properties: adaptability, reproducibility and modularity. In the following, these properties will be discussed in an application-oriented environment.

As an example, let us consider a semi-arid environment. It is characterized by two seasons: a dry season and a wet season [Amitrano et al., 2014]. During the dry season, the environment is almost completely dry and the vegetation reaches its minimum. During the wet season, heavy rainfalls cause a strong growth of vegetation and abundant water availability. In these particular climatic conditions, it could be very interesting to evaluate the scene dynamics with respect to a suitable reference situation, i.e. an image acquired at the peak of the dry season, in a change detection framework.

In Figure 4, we show a change-detection-oriented Level-1 $\alpha$  RGB composite (see Amitrano et al. [2015] for further details on this class of products) shooting the same scene depicted in Figure 1 and Figure 2. We can argue that this product is more understandable with respect to those previously shown, even without a technical expertise in SAR imagery. In fact, colors are helpful to understand things, especially if they are close to our everyday experience. In fact, we can associate, as an example, the blue color to water surfaces, or the green color to vegetation.

This association color-object is physical-based, and can be understood by analyzing the product composition. A reference image (April 2009, peak of the dry season) has been loaded on the blue band. A test image, (August 2010, wet season), has been loaded on the green band. The red band is reserved to the interferometric coherence.

This information allows for understanding colors. As an example, vegetation is green due to volumetric scattering triggered by vegetation growth during the wet season [Fung, 1979]. In the basin area, water coverage during the wet season causes a strong dominance of the dry season image (loaded on the blue band). That is why (seasonal) water appears in blue color. The balance between green and blue colors indicates stable features. As an example, water surfaces present in both the reference and test acquisitions are displayed in black (see the area at the center of Fig. 4). Trees are rendered in cyan due to a significant contribution of both blue and green bands. Bare soils exhibit a lower backscattering, therefore they have been rendered approximatively in Prussian blue (RGB code: 0,49,83). Man-made structures (usually characterized by high and stable backscattering and high interferometric coherence due to their phase stability) are depicted as bright targets.

The usefulness of Level-1 $\alpha$  representation in operative contexts can be confirmed only if the colorimetric response is stable varying the scene and the climatic conditions.

In Figure 5, a Level-1 $\alpha$  product concerning a southern Italy scene, characterized by a temperate Mediterranean climate, is shown. The reference image (blue band) has been acquired on December 2009. The test image (green band) has been acquired on August 2010.

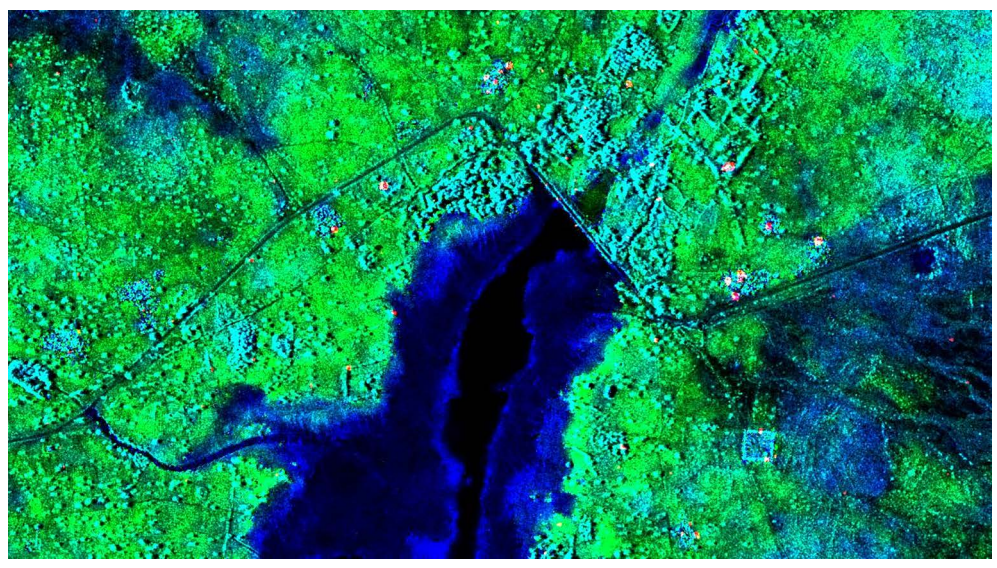


**Figure 4 - Burkina Faso, multitemporal RGB Level-1 $\alpha$  product. Red band: interferometric coherence. Green band: August 2010 (test image). Blue band: April 2009 (reference image).**

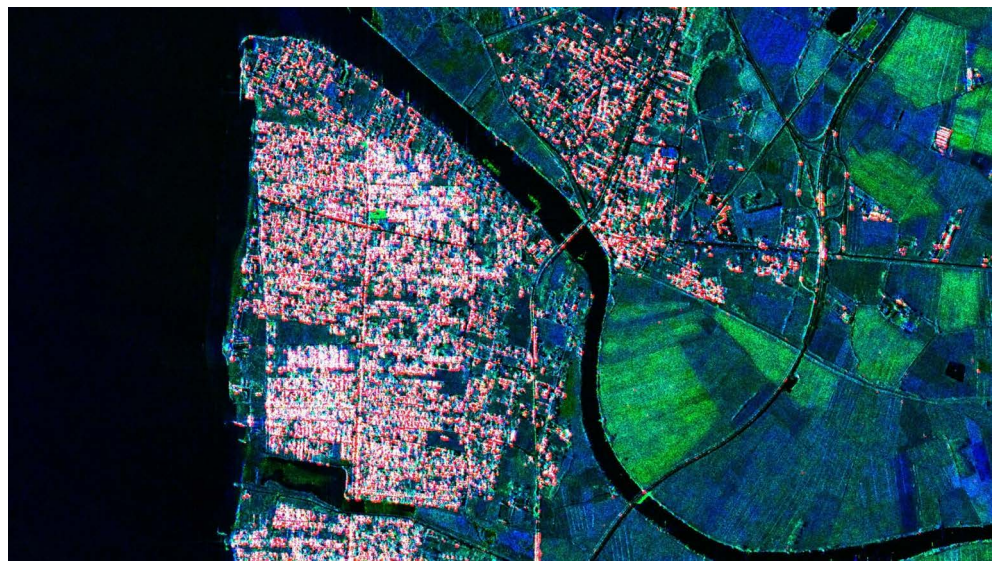


**Figure 5 - Castel Volturno (Italy), multitemporal RGB Level-1 $\alpha$  product. Red band: interferometric coherence. Green band: August 2010 (test image). Blue band: December 2009 (reference image).**

The reader should appreciate how the colorimetric response of the product is stable for a given phenomenon. In fact, we can observe, as an example, growing vegetation in green, sea surface in black, unchanged land cover in Prussian blue, built-up areas in white. This color-object association is perfectly consistent with the considerations made above for the Burkina Faso (semi-arid) scene.

### *Adaptive processing*

Previously, we discussed how to obtain a bi-temporal, change-detection-oriented Level-1 $\alpha$  RGB composite extracted from a series of  $N$  images. However, it is possible to combine these images in a unique RGB frame taking into account of some temporal indicators, such as the variance, the mean backscattering, the mean interferometric coherence, and the normalized saturation index [Amitrano et al., 2016]. In such way, a classification-oriented product can be obtained.

The result of this processing is depicted in Figure 6. We will refer to it as Level-1 $\beta$  product [Amitrano et al., 2016]. The red band is reserved to the time series variance. The green band is reserved to the mean backscattering. The blue band is given by a combination of the mean interferometric coherence and of the normalized saturation index. In particular, the mean interferometric coherence is shown when it is higher than a user-defined threshold (a value of 0.35 is reasonable). Otherwise, the blue band displays the saturation index, which is related to the maximum backscattering span calculated pixel-wise.

As for Level-1 $\alpha$  products, the aim is to provide an image favoring visual data mining through a physical-based, stable, color-object association close (for some features) to that expected by the observer.

As an example, the sea surface is rendered in almost pure blue color due to Bragg scattering. If the water is more stagnant, then the composition turns to black due to the low (and regular) backscattering. Changing land cover is characterized by pink or yellow color. In this case, it can be associated to growing crops. This is due to high contributions of the variance and/or of the saturation index.

Unchanged land cover is characterized by a negligible contribution of variance and of the saturation index. In Figure 6, areas characterized by dominant green component are associable to grasslands. For this feature, the rendering is thus almost consistent with the natural color palette. Finally, man-made structures are depicted in cyan due to their high (and stable) backscattering and their stability with respect to phase, which results in high values of the mean interferometric coherence.

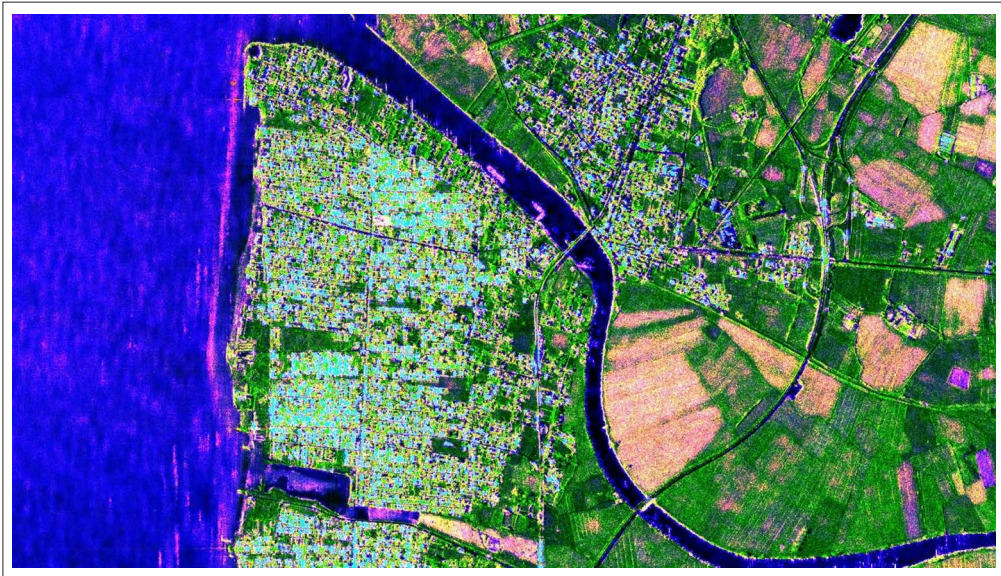


**Figure 6 - Castel Volturno (Italy), multitemporal RGB Level-1 $\beta$  product. Red band: time series variance. Green band: mean backscattering. Blue band: mean interferometric coherence combined with the saturation index.**

## Applications

Applications are the purpose of any remote sensing processing chain. When data come to end-users, they are usually combined with other geospatial data to address a specific practical problem. This combination is usually made in a GIS environment [Campbell and Wynne, 2011].

Therefore, it is fundamental that remote sensing data are provided in such way they can be analyzed in this kind of environment, and treated with the tools that are usually implemented within it. It is quite clear that SAR data are poorly suited to be processed with GIS. However, the introduction of Level-1 $\alpha$  and Level-1 $\beta$  products allows for changing this perspective. The following Sections are devoted to show how these products can be exploited in a GIS, with reference to both pixel-based and object-based image analysis.

### ***Pixel-based image analysis***

The world of applications is often populated by multidisciplinary users, with basic expertise in remote sensing (usually optical), and a poor background in electromagnetics. As discussed in the previous Sections, the use of RGB images in which the association color-object is close to everyday experience, or at least stable, should make SAR data more attractive for this class of users.

Another fundamental aspect for end-users is the possibility to process images with standard algorithms for information extraction. A non-expert user rarely implements his/her own code, preferring to exploit some ready-to-use solution. Many algorithms proposed in the recent SAR literature, although outstanding in terms of declared performances, are not manageable by multidisciplinary users due to the technical expertise necessary to set the required parameters. Moreover, they are very hard to find, being often not implemented in software suites or distributed in other ways.

The major software suites (both commercial and open source) implement only very robust and consolidated techniques. Therefore, when a new product is introduced, it is highly desirable that it is suitable to be treated with such algorithms. As an example, if we consider the commercial suite ENVI, only basic classifiers are implemented, such as the parallelepiped or maximum likelihood, as for supervised classifiers, or the k-means, as for unsupervised ones. These algorithms usually give unsatisfying results when applied to SAR data. However, these are the tools which are usually exploited for data analysis in the end-user community, representing another obstacle to SAR data diffusion.

The proposed products should mitigate this problem, being fully compatible with such algorithms [Amitrano et al., 2016b]. In the following, we will show how to effectively exploit Level-1 $\alpha$  products in a practical classification problem.

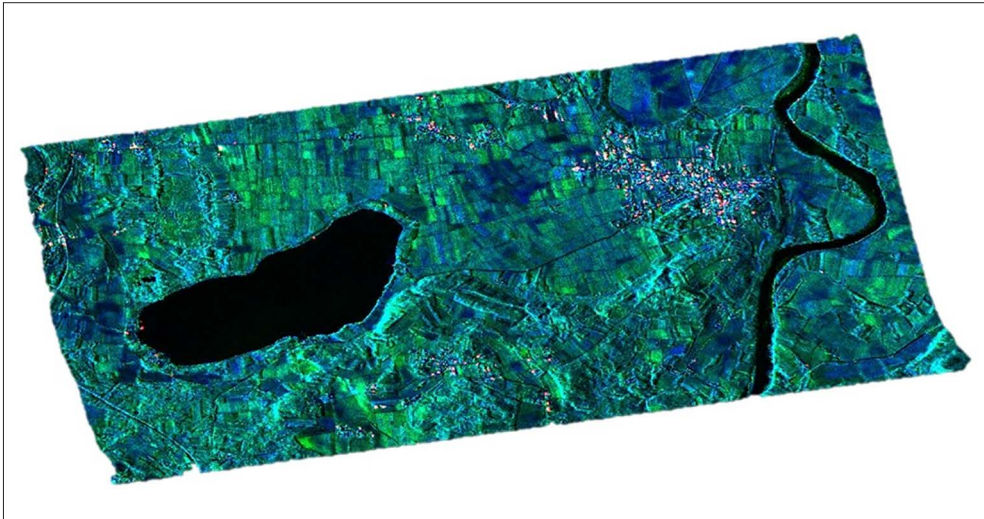


**Figure 7 - Vercelli area (Italy), Level-1 product. Reference image: 24 October 2008, test image: 12 November 2008. Product resolution 3m x 3m.**

The study area is depicted in Figure 7. It concerns a rural area in northern Italy, near the city of Vercelli. The product resolution is about 3m x 3m. The most relevant features of the scene are the Dorea Baltea river, the small city of Vische in its nearby and the Candia lake at West. The objective is to classify this scene using a very simple rule. The k-means algorithm is implemented in all the major software suites for remote sensing data analysis, both commercial (ENVI, ERDAS Imagine) and open source (ESA Sentinel-1 Toolbox, R). Therefore, it represents a suitable benchmark to test the reliability of the proposed RGB products with a class of algorithm very popular among users due to its availability and ease of use.

In Figure 8a, we show a 4-classes k-means clustering of the study area. In Figure 8b, the corresponding photo-interpreted ground truth image is shown. The considered classes are: “Water/weak scatterers”, “Built-up/Layover”, “Growing vegetation” and “Stable vegetation”. The registered accuracy for this classification is 86.34%. The kappa coefficient is  $\kappa = 0.76$ . The full confusion matrix is reported in Table 1.

From this table, it arises that there is a strong interclass confusion between the classes “Growing vegetation” and “Stable vegetation”. This was expected. In fact, the reference and test images have been acquired with a time span of just a couple of weeks. Therefore, the class “Growing vegetation” has, on average, a response very similar to stable vegetation. The class “Water/weak scatterers” is identified with the highest degree of accuracy due to its response very well separated from that of the other classes.

**Table 1 - 4-class confusion matrix for the k-means classification of the study area. Overall accuracy: 86.34%. kappa coefficient: 0.76.**

	Unclassified	Water/Weak	Built-up/Lay.	Grow. veg.	Stable veg.
Unclassified	99.99			2.6	
Water/Weak		98.77	6.47	1.23	10.5
Built-up/Layover		0.02	58.12	5.33	2.01
Growing vegetation	0.01	0.04	20.34	50.34	13.95
Stable vegetation	0.01	1.16	15.08	40.49	73.53
User accuracy		61.85	46.66	70.11	70.07
Producer accuracy		98.77	58.12	50.34	73.53

The class “Built-up” also shows a high percentage of errors. In fact, in the k-means classification, this class just refers to built-up features. Conversely, the ground truth refers to the urban area, in which the built-up feature is aggregated to other land cover (such as shadows, roads or grasslands). However, a pixel-based classifier (even more refined) can not evaluate relation of proximity and adjacency. Object-based image analysis (OBIA) is a valid solution to improve the classification results through the evaluation of geometric and topologic characteristics of the scene objects.

### ***Object-based image analysis***

OBIA (see Blaschke [2010] for an extended review) is widely exploited in the end-user community since it is implemented in many GIS software. Among them, eCognition is probably the most powerful and popular [Benz and Pottier, 2001; Flanders et al., 2003; Meinel and Neubert, 2004].

The possibility to operate with objects is related to the reliability of segmentation [Nagao and Matsuyama, 1980; Matsuyama and Hwang, 1990]. Some algorithms are implemented in eCognition, generally producing over-segmented images [Tzotsos et al., 2008]. Feature extraction process from such images is dictated by application. In the following, we consider two applications: river morphology [Mangelsdorf et al., 2013] and urban area mapping.

In river morphology, it is fundamental to extract precisely the stream contours, which is prior to the calculation of its geomorphological parameters [Demarchi et al., 2016]. Rivers are a sub-category of the macro-class “Water/Weak scatterers” we previously defined. In Level-1 $\alpha$  imagery, this class is mainly associable to the black color (in the case of permanent rivers).

Two strategies are possible: i) use eCognition segmentation tools or ii) exploit the k-means clustering previously performed. In this case, given the high accuracy of the k-means classification for this class, we can follow the second option, thus avoiding to deal with an over-segmented image. Therefore, we use as a preliminary mask the blue cluster (corresponding with the class “Water/Weak scatterers”) of the segmentation map shown in Figure 8a.

In such mask, there are two dominant features, i.e. the river and the lake. In order to separate them, the development of a rule set, which is essentially a knowledge-based expert system [Nagao and Matsuyama, 1980; Matsuyama and Hwang, 1990], is now in order.

The definition of this rule set is guided by simple geometric and spatial considerations. As an example, the river has well defined geometric properties, i.e. it is a very elongated and thin object. Using eCognition, these properties can be evaluated using the parameters *length of the mean line* and *density*. The first one evaluates the length of the mean line of objects’ skeletons. The second one describes the distribution in space of the pixels of an image object. The more an object is shaped like a filament, the lower its density. More details about these shape parameters can be found in Trimble Germany GmbH [2014].

Based on these considerations, a suitable rule set for the extraction of the class “River” is the following:

$$River : \begin{cases} Density < 1 \\ Length\ of\ the\ mean\ line > 1000\ pixels \end{cases} \quad [1]$$

The result of the application of this rule set to the mask constituted by the blue cluster of Figure 8 is depicted in Figure 9, where the Dora Baltea river is identified by the green contour.

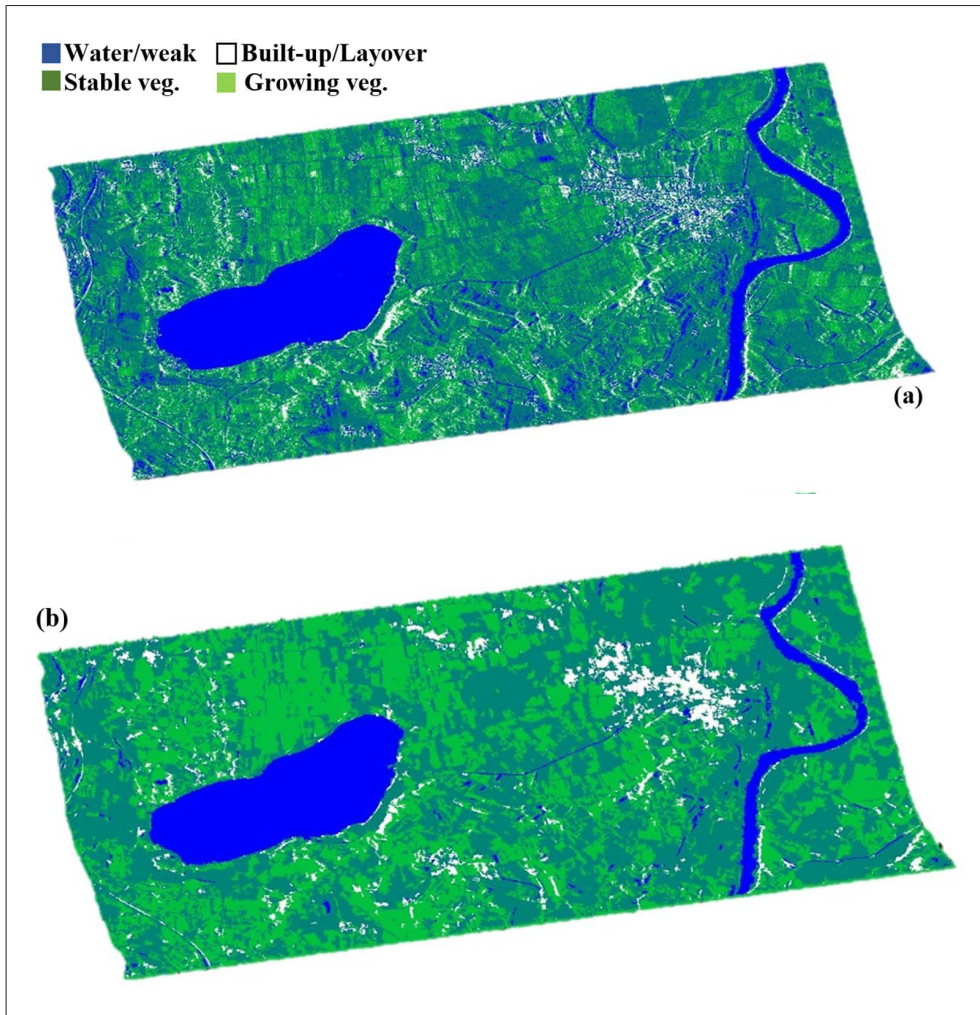


Figure 8 - (a) 4-class k-means classification, and (b) photo-interpreted ground truth image.

Similar considerations can be made to extract the “Lake” class. In this case, another shape parameter can be considered, i.e. the width with respect to the main line, which is defined as the average height of the triangles created by a Delaunay mesh and crossed by the mean line. Using this parameter in combination with the *density*, a suitable rule set for the extraction of the lake contour is:

$$River : \begin{cases} Density > 1 \\ Width > 100 \text{ pixels} \end{cases} \quad [2]$$

The results of the application of this rule set to the mask constituted by the blue cluster of Figure 8 is depicted in Figure 9, where the lake is identified by the yellow contour. In the following, the urban area extraction application is faced.

Urban areas are very heterogeneous environments, including different kind of land cover. This poses a problem about the definition of an urban area from a remote sensing point of view [Weeks, 2010]. As stated in Potere et al. [2009], currently, no generally accepted definition of “urban land” exists, because in any case it involves some arbitrary decisions in finding boundaries, which tend to merge physically and functionally with their neighbor [Boehm and Schenkel, 2006].

A suitable workflow for mapping urban areas could start by identifying the principal feature of this class, which is the built-up area, and then grow it by fusion with neighbor objects thorough a suitable rule set. Therefore, the most important parameter to take into account in this activity is constituted by the spatial relationships between objects.

Using eCognition, we exploited the multiresolution segmentation tool [Trimble Germany GmbH, 2014] to segment the RGB image. As expected, we obtained an oversegmented image with more than 5 million of objects. Therefore, the challenge is to develop a rule set suitable with our purpose and to manage such a high number of objects.

As aforementioned, we propose to identify the built-up feature, and then grow the urban area around it. In Level-1 $\alpha$  RGB composites, the built-up area is typically rendered in white color, due to the high contribution of all the involved channels [Amitrano et al., 2016a]. Therefore, using eCognition, we can set the following conditions:

- Condition 1: Assign class “built-up” if  $\hat{R} > 50$  and  $\hat{G} > 150$  and  $\hat{B} > 150$ .
- Condition 2: Assign class “urban area” to each object whose center of mass is placed at a distance lower than  $t_1$  pixels (or meters) from an object belonging to the “built-up” class.
- Condition 3: Assign class “urban area” to each object sharing its border with an “urban area” object with a percentage higher than  $t_2$ .
- Condition 4: Reject object classified as “urban area” smaller than  $t_3$  pixels (or square meters).

We indicated with the symbol  $\hat{\cdot}$  the mean calculated within a segment, and with R, G and B the red, green and blue band of the Level-1 $\alpha$  composite, respectively.

Condition 1 indicates that built-up feature is represented by bright targets. The other statements aim at analyzing the spatial relations between built-up objects and the surrounding area in order to retrieve the “urban area” class.

In Condition 2, the “urban area” class is initialized by growing the areas surrounding the built-up feature. This condition is governed by the parameter  $t_1$ , which rules the amount of the growth. It is related to the dimension of the city we are considering and to the spatial resolution. In fact, it can be assumed that the larger the city, the larger the area it influences, i.e. the larger the area that can be considered urban even if it is not covered by any built-up feature. In the considered study area, only very small cities are present, thus this parameter should be small, as an example in the order of 10 pixels (i.e. 30 meters).

Condition 3 allows for growing the retrieved urban area around the relevant objects and filling small holes within them. The concept governing this rule is that if an object shares a significant percentage of its perimeter with an urban area, it should be considered urban, as well. This is the case, an example, of a city park, or, in general, of areas surrounded by urban structures.

Condition 4 is ruled by the size of the urban agglomerates which the analyst wants to map. In this case, regions smaller than 2000 pixels (about 20000 m<sup>2</sup>) have been excluded from the analysis.

In Figure 9, the retrieved urban area map is shown with a red contour, and superimposed to the input RGB product. The reader should note how it develops around the denser built-up features, including several land cover which are considered integral part of the cities because of their vicinity to urban infrastructures.

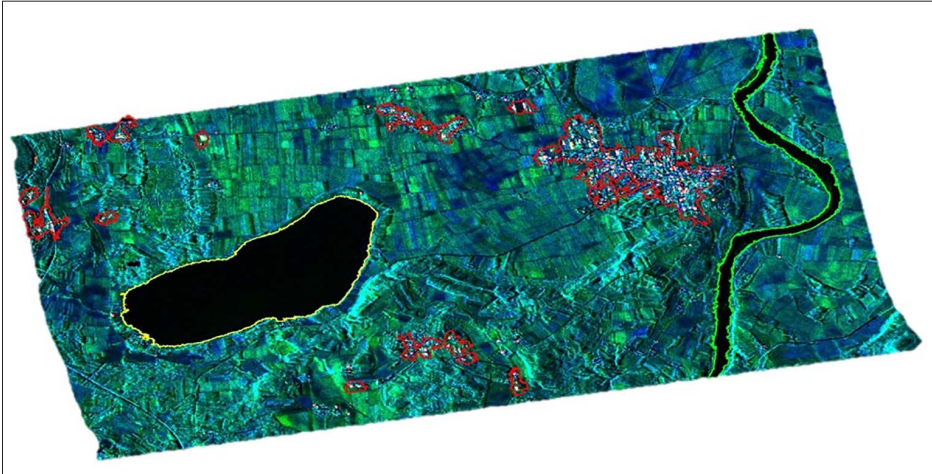


Figure 9 - Urban area contour (in red), river contour (in green), and lake contour (in yellow) output by the OBIA superimposed to the input Level-1a product.

In Figure 10, the final classification map is shown. The retrieved urban areas are depicted in magenta color. Moreover, with respect to the map outputted by the k-means algorithm (see Fig. 8a), we added the classes “River” and “Lake” previously discussed, for a total of 7 classes. The confusion matrix for this classification is reported in Table 2. The obtained  $k$  coefficient and overall accuracy are of 0.77 and 86.3%, respectively.

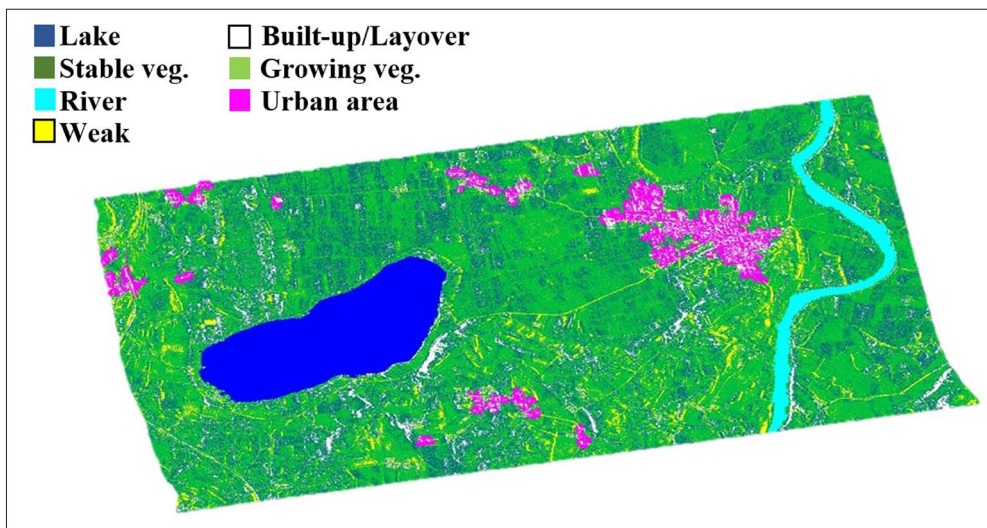


Figure 10 - Final 7-class classification map.

**Table 2 - 7-class confusion matrix for the object-based classification of the study area. Overall accuracy: 86.3%. kappa coefficient: 0.77.**

	Unclassified	Lake	Grow. veg.	Stable veg.	Built-up	Weak	Urban	River
Unclassified	99.98			2.61			0.14	
Lake		99.66	0.06		0.02	5.23		
Grow. veg.	0.01	0.23	74.44	40.65	3.65	9.66	19.96	2.41
Stable veg.	0.01	0.06	13.85	50.37	13.03	0.28	9.42	0.38
Built-up/Lay.		0.04	1.64	5.18	58.14	0.22	9.37	0.1
Weak		0.01	9.33	1.16	1.31	77.92	5.51	0.14
Urban	0.01		0.53	0.03	23.85	0.41	55.6	
River			0.14		0.01	6.27		96.96
User acc.	99.35	99.03	69.24	70.9	46.64	11.29	57.32	94.08
Prod. acc.	99.98	99.66	74.44	50.37	58.14	77.92	55.6	96.96

From Table 2, it arises a high correspondence between the photo-interpreted ground truth image and the classes “Lake” and “River”. As expected, a moderate interclass confusion is found for the classes “Growing vegetation” and “Stable vegetation”, as well as for the classes “Urban” and “Built-up”. In particular, in the class “Urban” fall pixels belonging to all the other classes of the ground truth (except those belonging to the classes “Lake” and “River”) with percentage higher than 5%. This is understandable due to the arbitrariness with whom the borders of the cities are traced in the ground truth.

### Conclusions

In this paper, we introduced a new end-user framework for color representation of SAR data. Its aim is to lower the expertise required to manage data, providing intermediate products between the classic Level-1 and Level-2, whose principal characteristics are interpretability, reproducibility and possibility to be processed with simple algorithms.

Two classes of products were discussed. Level-1 $\alpha$  products are bi-temporal products obtained from multitemporal processing of  $N$  images. They are particularly well suited for change-detection applications with respect to a reference situation, whose selection should be application-oriented in order to obtain the best visual experience and physical consistence with the case study.

Level-1 $\beta$  products synthetize in a unique RGB frame the dynamics of the scene expressed by  $N$  images. Therefore, these products are particularly oriented toward classification applications. As for Level-1 $\alpha$  imagery, a proper selection of the bands and of their disposition allows for obtaining well-balanced RGB composites. For some features, the rendering in the natural color palette is possible, and this favors users’ experience.

Both Level-1 $\alpha$  and Level-1 $\beta$  products can be treated with simple algorithms for information extraction. We tested the suitability of these products with applicative scenarios through the implementation of two simple classification activities. In the first case, pixel-based unsupervised k-means, 4-class clustering was performed. A satisfying agreement with the available ground truth, in terms of the standard classification quality indicators, was registered.

In the second case, we implemented an object-based image analysis to split some of the classes retrieved through the pixel-based classification into more significant categories. Shape parameters have been exploited to separate the river from the lake and other weak scatterers present on the scene. Even in this case, the obtained results showed a good agreement with the available ground truth.

The characteristics of the RGB products discussed in this paper are particularly oriented towards the end-user community and could represent a good mean to favor the diffusion of SAR data in multidisciplinary contexts.

## References

- Amitrano D., Belfiore V., Cecinati F., Di Martino G., Iodice A., Mathieu P.-P., Medagli S., Poreh D., Riccio D., Ruello G. (2016a) - *Urban areas enhancement in multitemporal SAR RGB images using adaptive coherence window and texture information*. IEEE Journal of Selected Topics on Applied Earth Observations and Remote Sensing, 9: 3740-3752. doi: <http://dx.doi.org/10.1109/JSTARS.2016.2555340>.
- Amitrano D., Cecinati F., Di Martino G., Iodice A., Mathieu P.-P., Riccio D., Ruello G. (2016) - *Multitemporal Level-1 $\beta$  Products: Definitions, Interpretation, and Applications*. IEEE Transactions on Geoscience and Remote Sensing, 54 (11): 6545-6562. doi: <http://dx.doi.org/10.1109/TGRS.2016.2586189>.
- Amitrano D., Di Martino G., Iodice A., Riccio D., Ruello G. (2015) - *A New Framework for SAR Multitemporal Data RGB Representation: Rationale and Products*. IEEE Transactions on Geoscience and Remote Sensing, 53: 117-133. doi: <http://dx.doi.org/10.1109/TGRS.2014.2318997>.
- Amitrano D., Di Martino G., Iodice A., Riccio D., Ruello G. (2016b) - *An end-user oriented framework for the classification of multitemporal SAR images*. International Journal of Remote Sensing, 37: 248-261.
- Amitrano D., Di Martino G., Iodice A., Ruello G., Ciervo F., Papa M.N., Koussoube Y. (2014) - *Effectiveness of high-resolution SAR for water resource management in low-income semi-arid countries*. International Journal of Remote Sensing, 35: 70-88. doi: <http://dx.doi.org/10.1080/01431161.2013.862605>.
- Benz U., Pottier E. (2001) - *Object based analysis of polarimetric SAR data in alpha-entropy-anisotropy decomposition using fuzzy classification by eCognition*. Proceedings of the IEEE International Geoscience and Remote Sensing Symposium, pp. 1427-1429. doi: <http://dx.doi.org/10.1109/igarss.2001.976867>.
- Blaschke T. (2010) - *Object based image analysis for remote sensing*. ISPRS Journal of Photogrammetry and Remote Sensing, 65: 2-16. doi: <http://dx.doi.org/10.1016/j.isprsjprs.2009.06.004>.
- Boehm C., Schenkel R. (2006) - *Analysis of Spatial Patterns of Urban Areas Using High Resolution Polarimetric SAR*. Proceedings of the 1st EARSel Workshop of the SIG Urban Remote Sensing.
- Campbell J.B., Wynne R.H. (2011) - *Introduction to Remote Sensing*. The Guilford Press, New York.
- Datcu M., Seidel K. (2005) - *Human Centered Concepts for Exploration and Understanding of Earth Observation Images*. IEEE Transactions on Geoscience and Remote Sensing, 43: 52-59. doi: <http://dx.doi.org/10.1109/TGRS.2005.843253>.

- De Grandi G.F., Leysen M., Lee J.S., Schuler D. (1997) - *Radar reflectivity estimation using multiple SAR scenes of the same target: technique and applications*. Proceedings of the IEEE International Geoscience and Remote Sensing Symposium, pp. 1047-1050. doi: <http://dx.doi.org/10.1109/igarss.1997.615338>.
- Dellepiane S.G., Angiati E. (2012) - *A New Method for Cross-Normalization and Multitemporal Visualization of SAR Images for the Detection of Flooded Areas*. IEEE Transaction on Geoscience and Remote Sensing, 50: 2765-2779. doi: <http://dx.doi.org/10.1109/TGRS.2011.2174999>.
- Demarchi L., Bizzi S., Piégay H. (2016) - *Hierarchical object-based mapping of riverscape units and in-stream mesohabitats using LiDAR and VHR imagery*. Remote Sensing, 8 (2): 97. doi: <http://dx.doi.org/10.3390/rs8020097>.
- Di Martino G., Poderico M., Poggi G., Riccio D., Verdoliva L. (2014) - *Benchmarking Framework for SAR Despeckling*. IEEE Transactions on Geoscience and Remote Sensing, 52: 1596-1615. doi: <http://dx.doi.org/10.1109/TGRS.2013.2252907>.
- Fischer W.A., Hemphill W.R., Kover A. (1976) - *Progress in remote sensing (1972-1976)*. Photogrammetria, 32: 33-72. doi: [http://dx.doi.org/10.1016/0031-8663\(76\)90013-2](http://dx.doi.org/10.1016/0031-8663(76)90013-2).
- Flanders D., Hall-Beyer M., Pereverzoff J. (2003) - *Preliminary evaluation of eCognition object-based software for cut block delineation and feature extraction*. Canadian Journal of Remote Sensing, 29: 441-452. doi: <http://dx.doi.org/10.5589/m03-006>.
- Fung A.K. (1979) - *Scattering from a Vegetation Layer*. IEEE Transactions on Geoscience Electronics, 17: 1-6. doi: <http://dx.doi.org/10.1109/TGE.1979.294601>.
- Infoterra (2014) - *Radiometric Calibration of TerraSAR-X Data*. Available online at: [http://www2.geo-airbusds.com/files/pmedia/public/r465\\_9\\_tsx-x-itd-tn-0049-radiometric\\_calculations\\_i3.00.pdf](http://www2.geo-airbusds.com/files/pmedia/public/r465_9_tsx-x-itd-tn-0049-radiometric_calculations_i3.00.pdf) Accessed 1.4.16).
- Jacobson N.P., Gupta M.R., Cole J.B. (2007) - *Linear Fusion of Image Sets for Display*. IEEE Transactions on Geoscience and Remote Sensing, 45: 3277-3288. doi: <http://dx.doi.org/10.1109/TGRS.2007.903598>.
- Madhok V., Landgrebe D.A. (2002) - *A Process Model for Remote Sensing Data Analysis*. IEEE Transactions on Geoscience and Remote Sensing, 40: 680-686. doi: <http://dx.doi.org/10.1109/TGRS.2002.1000327>.
- Mangelsdorf J., Scheurmann K., Weiss F.H. (2013) - *River morphology: a guide for geoscientists and engineers*. Springer, Berlin, Heidelberg.
- Marr D. (1982) - *Vision*. W. H. Freeman, San Francisco.
- Martinez J., Le Toan T. (2007) - *Mapping of flood dynamics and spatial distribution of vegetation in the Amazon floodplain using multitemporal SAR data*. Remote Sensing of Environment, 108: 209-223. doi: <http://dx.doi.org/10.1016/j.rse.2006.11.012>.
- Matsuyama T., Hwang V.S.-S. (1990) - *SIGMA - A Knowledge-Based Aerial Image Understanding System*. Plenum Press, New York.
- Meinel G., Neubert M. (2004) - *A comparison of segmentation programs for high resolution remote sensing data*. The International Archive of the Photogrammetry, Remote Sensing and Spatial Information Science, 35: 1097-1105.
- Nagao M., Matsuyama T. (1980) - *A Structural Analysis of Complex Aerial Photographs*. Plenum Press, New York. doi: <http://dx.doi.org/10.1007/978-1-4615-8294-6>.
- Potere D., Schneider A., Angel S., Civco D. (2009) - *Mapping urban areas on a global scale: which of the eight maps now available is more accurate?* International Journal of

- Remote Sensing, 30: 6531-6558. doi: <http://dx.doi.org/10.1080/01431160903121134>.
- Trimble Germany GmbH (2014) - *eCognition Reference Book*. Munich.
- Tzotsos A., Iosifidis C., Argiald D. (2008) - *A hybrid texture-based and region based multi-scale image segmentation algorithm*. In: Blaschke T., Lang S., Hay G. (Eds.), *Object-Based Image Analysis: Spatial Concepts for Knowledge-Driven Remote Sensing Applications*, Springer-Verlag, Berlin, Heidelberg. doi: [http://dx.doi.org/10.1007/978-3-540-77058-9\\_12](http://dx.doi.org/10.1007/978-3-540-77058-9_12).
- Weeks J.R. (2010) - *Defining Urban Areas*. In: Rashed T., Jurgens C. (Eds.), *Remote Sensing of Urban and Suburban Areas*, Springer, Berlin. doi: [http://dx.doi.org/10.1007/978-1-4020-4385-7\\_3](http://dx.doi.org/10.1007/978-1-4020-4385-7_3).

© 2016 by the authors; licensee Italian Society of Remote Sensing (AIT). This article is an open access article distributed under the terms and conditions of the Creative Commons Attribution license (<http://creativecommons.org/licenses/by/4.0/>).